Hindawi
Geofluids
Volume 2018, Article ID 9461214, 19 pages
https://doi.org/10.1155/2018/9461214

Research Article

High-Resolution Wellbore Temperature Logging Combined with a Borehole-Scale Heat Budget: Conceptual and Analytical Approaches to Characterize Hydraulically Active Fractures and Groundwater Origin

Guillaume Meyzonnat,[1] **Florent Barbecot**,[1] **José A. Corcho-Alvarado**,[2] **Antoine Tognelli**,[3] **Hermann Zeyen**,[4] **Alexandra Mattei**,[1,5] **and Renald McCormack**[6]

[1]*Department of Earth and Atmospheric Sciences, Geotop-UQAM, Montréal, QC, Canada*
[2]*Spiez Laboratory, Federal Office for Civil Protection, Spiez, Switzerland*
[3]*CEA, DAM, DIF, F-91297 Arpajon, France*
[4]*Department of Earth Sciences, GEOPS Laboratory, Paris-Saclay University, Paris-Sud University, CNRS, Orsay, France*
[5]*MINES Paris Tech, Paris, France*
[6]*Envir'Eau-Puits Inc., Saint-Nicolas, QC, Canada*

Correspondence should be addressed to Guillaume Meyzonnat; meyzonnat.guillaume@uqam.ca

Received 29 June 2017; Revised 18 October 2017; Accepted 20 February 2018; Published 3 April 2018

Academic Editor: Walter A. Illman

This work aims to provide an overview of the thermal processes that shape wellbore temperature profiles under static and dynamic conditions. Understanding of the respective influences of advection and conduction heat fluxes is improved through the use of a new heat budget at the borehole scale. Keeping in mind the thermal processes involved, a qualitative interpretation of the temperature profiles allows the occurrence, the position, and the origin of groundwater flowing into wellbores from hydraulically active fractures to be constrained. With the use of a heat budget developed at the borehole scale, temperature logging efficiency has been quantitatively enhanced and allows inflow temperatures to be calculated through the simultaneous use of a flowmeter. Under certain hydraulic or pumping conditions, both inflow intensities and associated temperatures can also be directly modelled from temperature data and the use of the heat budget. Theoretical and applied examples of the heat budget application are provided. Applied examples are shown using high-resolution temperature logging, spinner flow metering, and televiewing for three wells installed in fractured bedrock aquifers in the St-Lawrence Lowlands, Quebec, Canada. Through relatively rapid manipulations, thermal measurements in such cases can be used to detect the intervals or discrete positions of hydraulically active fractures in wellbores, as well as the existence of ambient flows with a high degree of sensitivity, even at very low flows. Heat budget calculations at the borehole scale during pumping indicate that heat advection fluxes rapidly dominate over heat conduction fluxes with the borehole wall. The full characterization of inflow intensities provides information about the distribution of hydraulic properties with depth. The full knowledge of inflow temperatures indicates horizons that are drained from within the aquifer, providing advantageous information on the depth from which groundwater originates during pumping.

1. Introduction

Aquifer hydraulic properties are most commonly determined through pumping and slug tests. These techniques provide fast and reliable measurements of mean transmissivity and effective porosity, which often yield sufficient information to manage groundwater resources in terms of productivity. However, for applications where solute transport processes cannot be neglected (i.e., wellhead protection area delineation, contaminated site remediation), the knowledge of mean hydraulic parameters alone is insufficient, and groundwater flow paths need to be assessed. Hydrogeologists always

have to deal with a certain degree of spatial heterogeneity, because aquifer architectures originate from complex geological processes (i.e., sedimentology, tectonics), which generate heterogeneous [1] and scale-dependent patterns [2]. Despite the heterogeneous nature of aquifers, the use of borehole logging techniques to address this heterogeneity remains uncommon. For instance, pumping tests usually carried out for drinking water supply wells do not typically address the vertical variability of the production zones within the boreholes [3]. Since the most common borehole logging technique, known as the packer test, is more difficult to implement, more time-consuming, and thus more expensive than usual pumping tests, the vertical investigation of aquifer heterogeneities is still rare in hydrogeological surveys.

The heterogeneous nature of aquifers has been investigated and highlighted worldwide. In the Canadian context of this study, examples dealing with aquifer heterogeneity have been provided for both granular [4] and fractured [5] matrices. Nastev et al. [6] described the lognormal decrease of hydraulic conductivities with depth in postglacial fractured bedrock in Quebec, Canada. Recent regional groundwater characterizations, also carried out in Quebec, between 2008 and 2015, included the investigation of vertical bedrock fracturing patterns. These generally showed no correlation between well productivity and type of bedrock formation [7–9]. Packer tests and acoustic televiewing performed by Carrier et al. [7] showed that decreasing fracture densities are generally associated with decreasing hydraulic conductivities with depth. However, these results have high standard deviations, revealing strong vertical heterogeneities from one well to another. Indeed, packer tests performed for some wells in the same period [8, 9] did not reveal systematic decreases in bedrock fracturing with depth.

Other borehole logging techniques have garnered the attention of hydrogeologists over the last two decades. For instance, tracer experiments allow fluid velocities [10] or concentration dilution [11] to be measured following the injection of a tracer into boreholes during pumping, or tracer breakthrough in boreholes neighboring the injection well to be measured [12]. Spinner [13] or electromagnetic [14, 15] flowmeters allow water velocities to be measured very efficiently and directly inside the borehole with high spatial resolution. Such fluid velocity measurements inside boreholes during pumping allow the vertical distribution of the hydraulic properties of the surrounding rocks to be determined [13]. For the same application, but under low flow conditions, heat pulse flowmeters [15, 16] are especially useful to measure ambient borehole flow. Temperature logging in boreholes is another type of investigation technique. Applications specifically dedicated to hydrogeology make use of temperature logging in boreholes to estimate recharge rates [17–19], to trace local [20, 21] or regional [22] groundwater flows, or to infer the lateral heterogeneity of hydraulic properties for a section of an aquifer [23]. These applications typically address large-scale heat transport processes within the subsurface and/or involve heat transport processes over relatively long time scales.

At the borehole scale, high-resolution temperature profiling is of particular interest in hydrogeology, and its use has become more frequent over the last decade, coinciding with temperature sensor resolution improvement to 0.001°C. Hydrogeological information obtained from recent passive and/or active temperature measurement techniques [24, 25] are now capable of competing with other, more conventional investigation techniques (e.g., involving hydraulic packer tests or solute tracing) to provide valuable information about aquifer hydraulic and fracturing structure, used to infer groundwater flow paths.

Passive temperature measurements consist of logging temperature in a wellbore without introducing a heat source, so that obtained profiles only depend on natural hydrogeological conditions, thermal properties of the rock, and/or aquifer solicitation through pumping. For instance, the vertical distribution and interconnectivity of fractures in wellbores can be well-described by coupling flow and passive temperature measurements. Such examples are given by Chatelier et al. [26] and Le Borgne et al. [27], who have explicitly pointed out the advantage of combining passive temperature and flowmeter logs, where the passive temperature log gives the precise depth at which inflow occurs, and the flow log gives a precise measurement of the flow rate in the interval between inflow and outflow zones. Discussions of groundwater origin from identified fractures are also found in the literature. One such example is also provided by Chatelier et al. [26], by coupling passive temperature measurement and flow logs with elaborate in situ data. Other recent technical advances make it possible to measure instantaneous temperature profiles using optical fiber. This technology is often implemented with an active measurement of temperature by heating a section or the entire length of the water column. Pehme et al. [28] used active temperature measurements to detect lateral ambient flow through hydraulically active fractures by measuring the thermal recovery of the water column in the borehole after it was heated. In another example, Bense et al. [29] used a coaxial system of heating cable and optical fiber and then used the variation in temperature profiles during pumping to calculate the depth-flow distribution in wellbores.

Although these latter active technologies allow direct quantitative results, their setup remains rather delicate and time-consuming for in situ applications. Moreover, the effectiveness of the method is not guaranteed in all in situ cases, because the resolution of optical fiber temperature measurements (±0.5°C, or at best ±0.02°C with the use of the calibration baths) is still low compared with those of the current thermistors (±0.001°C), which are preferentially used for passive measurements. Thermal numerical modelling has been used by Klepikova et al. [30] and Klepikova et al. [31] to present the concepts and numerical methods behind the inversion of temperature profiles to flow profiles in wellbores, thus using the temperature probe as a high-resolution flowmeter. Previous work has made use of thermal analytical models, especially in the case of (low) ambient flows in wellbores for fractured media. An explicit thermal analytical solution considering a semi-infinite plane geometry was provided by Drury and Jessop [32] to model transient temperature shifts within the aquifer with increasing distance from the active fracture intercepting the wellbore. With an

application for ambient inflow, which flows through the wellbore, Ge [33] proposed a theoretical model to estimate both fluid flow velocity and temperature for a given inflow. Previous work has focused on experiments under thermal steady-state conditions during pumping and was generally applied at depth or at locations where the geothermal gradient is linear.

This study investigates the vertical distribution of hydraulic properties in fractured bedrock wells using flow metering and televiewing, but with a main focus on temperature borehole logging. As cited above, numerous works have already highlighted the pertinence of temperature logging to identify the occurrence and the positions of productive zones in wellbores. Through the introduction of a new heat budget model, this work aims to enhance the qualitative interpretation of depth-temperature profiles against advection and conduction fluxes at the borehole scale, across a range of static and dynamic conditions in fractured aquifers. The second objective is to enhance the potential of passive temperature logging to quantify flow and the temperature of inflows into boreholes with the use of a heat budget. Previous analytical models found in the literature typically allowed calculations for only a limited number of fractures (i.e., one or two fractures at best, in the case of ambient flows) and did not attempt to model the complete depth-temperature profile when several inflows occurred and mixed in the wellbore. The heat budget proposed in this work aims to model depth-temperature profiles for the entire wellbore length, for several inflows that mix in the borehole, and depending on pumping conditions (duration and discharge intensity). Simultaneous temperature measurement and flow metering are applied within the heat budget to quantify information about the origin of several groundwater inflows based on their temperature. The use of this analytical procedure is also theoretically investigated to test its potential to quantify both flow and temperature of inflows in wellbores through the single logging of depth-temperature profiles.

The following abbreviations are used throughout the text for brevity: the temperature of the water column measured in the borehole under ambient ($\mathbf{T_S}$) and under dynamic (i.e., pumping) ($\mathbf{T_D}$) conditions; the temperature of groundwater discharging into the borehole at depth ($\mathbf{T_i}$), originating from a discrete or distributed interval of hydraulically active fracture(s); and the temperature of the aquifer ($\mathbf{T_A}$), depending on depth as function of geothermal heat flux, seasonal and climatic variation of the soil surface temperature, regional groundwater circulation, and recharge fluxes, but excluding the influence of fluid advection due to the presence of a wellbore or the pumping thereof.

2. Materials and Methods

2.1. Site Description. The study area is located in southern Quebec, within two geological regions that correspond to the St. Lawrence Platform and the Appalachian Mountains (Figure 1). The Ordovician geological units of the St. Lawrence Platform are of sedimentary origin and consist of thick sequences of sandstone of the Potsdam Group, dolomite of the Beekmantown Group, limestone of the Chazy, Black River, and Trenton Groups, Utica shales, and mudstones of the Queenston Group. In the eastern part of the study area, the Appalachian range corresponds to complex, imbricated metamorphic thrust sheets produced during the Taconian Orogeny: slates with a bedded shaly matrix containing chaotic blocks of cherts, sandstone, and dolomitic schists. These geological units are represented in Figure 1 as a simplified version of the detailed mapping by Globensky [34]. The geomorphology of Quebec is marked by glaciation-deglaciation phases, with unconsolidated sediments of glacial and postglacial origin overlying the fractured bedrock. The complex stratigraphy of the unconsolidated sediment largely controls the hydrogeological context of the underlying fractured bedrock aquifers. In such a glacial geomorphological context, the unconformity between Quaternary unconsolidated sediment and the bedrock is very sharp, and bedrock fracturing generally decreases strongly with depth over the first hundred meters [7].

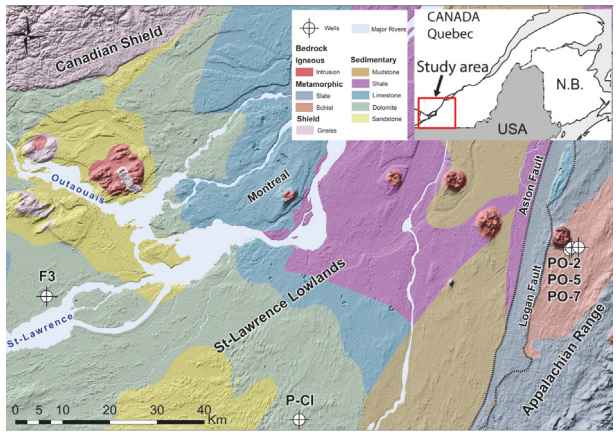

FIGURE 1: Location of wells in the current study and geological map.

Three (F3, P-Cl, and PO-7) of the five wells presented in Figure 1 have been studied in detail. PO-2 and PO-5 are only used as references for ambient temperature profiles with depth (see Section 4.2.1). All investigated wells have a 150 mm diameter, are steel-cased for the total thickness of unconsolidated sediment, and are anchored one meter into the bedrock. Below the steel tubing, boreholes are uncased. Well F3 has a total depth of 20.4 m and was drilled for a regional hydrogeological mapping study [35]. Sediment at this location consists of 4.3 m of Champlain silty-clays and 5.7 m of glacial till covering the bedrock. Sedimentary bedrock is Ordovician calcareous dolomite of the Beekmantown Group, Beauharnois Formation. The bedrock aquifer is confined under impermeable clay and till sediments, and a pumping test provided a transmissivity of 3.7×10^{-3} m^2/s and a productivity of approximately 287 L/min. The productivity is defined here as the maximum total discharge rate obtained when the drawdown in the wellbore has stabilized. Wells PO-7, PO-2, PO-5, and P-Cl were drilled for municipal groundwater investigation, and access to these wells was kindly provided by the lead hydrogeologist. Well PO-7 has a total depth of 61 m, a productivity of 340 L/min, and a transmissivity of 4.2×10^{-3} m^2/s. At this location, 8 m of

fine sand, including silty lenses, overlay the bedrock, which consists of red schists of the Cambrian Shefford Group, Mawcook Formation. Wells PO-2 (92 m depth; productivity 45 L/min) and PO-5 (91 m depth; productivity 15 L/min) are located 200 m and 1 km from well PO-7, respectively, within the same bedrock formation, with land cover, as well as the nature and thickness of the unconsolidated sediments varying only slightly. Well P-Cl has a total depth of 37 m and a productivity of 80 L/min. Glacial till less than 0.6 m thick overlies the bedrock, which consists of Ordovician dolomitic sandstone of the Beekmantown Group, Theresa Formation.

2.2. Borehole Logging with a Spinner Flowmeter and Televiewing. Water velocities in wells PO-7 and F3 were measured during pumping with a spinner flowmeter [36] operated with a winch controller [37]. Pumping rates were set to be as high as possible to maximize water velocities flowing into the borehole and thus maximizing flowmeter sensitivity. Discharge rates, however, were carefully constrained in order to avoid well dewatering below the base of the steel-casing, allowing measurements within the whole uncased section of the wellbores. The spinner flowmeter was calibrated for each well under static conditions, with winch down speeds varying from 1 to 3 m/min. During pumping tests, the pumps were placed at the top of the well and water velocities were logged with the spinner flowmeter trolled downward, in order to maximize fluid velocities and thus to maximize the flowmeter sensitivity. Measurements were performed at a resolution of 5 cm and a winch down speed of 2 m/min. Raw, noisy signals measured with the flowmeter were smoothed using a moving average of 10 measurements. Flow velocities were converted into flow rates by dividing the measured flow velocities by the section area of the borehole. Flow rates at depth were converted into a percentage of pumping discharge by dividing them by the total pumping rate. Total water discharged during pumping was measured with a volumetric counter placed at the hose outlet, and with bucket and chronometer, and compared with the total discharge measured with the flowmeter within the steel-casing. Discrepancies in the total discharge obtained by these two means were less than 5%. Fluid velocity measurements in the borehole during pumping were taken when steady state was reached (i.e., with residual drawdown of less than 1 cm/20 min). Pumping tests performed at different discharge rates for F3 and PO-7 did not reveal any variation in the vertical distribution of water inflows into the borehole measurable by the flowmeter. Televiewing with an optical borehole imager [38] was coupled with flowmeter measurements to better constrain the location and the discrete or distributed nature of hydraulically active fractures.

2.3. Passive Temperature Borehole Logging. Temperature profiles in water columns were measured with a 0.01°C resolution thermistor probe [39]. Measurements were always taken facing downward, with a maximum interval of one meter. For all temperature logging under dynamic conditions, the pump was placed at a shallow depth within the casing or just below the bottom of the casing, avoiding temperature disturbance and allowing space for the uncased length of the studied borehole. Static profiles were systematically taken before initiating measurements under pumping conditions. Depths to the water table under static conditions are shown in Figure 9(a). Discharge rates, as well as drawdown stabilized during pumping, are shown in Figures 9(b), 9(c), and 9(d) for wells PO-7, P-Cl, and F3, respectively. For a given well, all static and dynamic temperature logs were taken on the same day. Wells PO-2, PO-5, and PO-7 were installed in the same red schist formation and were drilled at a 200 m spacing. Wells PO-2 and PO-5 were not accessible for logging under dynamic conditions, but the presentation of their ambient temperature logs together with both the static and dynamic PO-7 logs is useful, because PO-2 and PO-5 reach greater depths (92 m).

2.4. Calculation of Hydraulic Properties from Velocity Logs. The distribution of horizontal hydraulic conductivity along the length of the borehole was obtained directly from flowmeter measurements. As described by Barahona-Palomo et al. [13], the hydraulic conductivity of each fractured zone (K_i) can be calculated using (1), where T is the total hydraulic transmissivity obtained from a pumping test, Q is the total pumping rate, and q_i is the inflow associated with the fracture zone interval of vertical thickness b_i.

$$K_i = \frac{1}{b_i}\frac{q_i}{Q}T. \quad (1)$$

3. Background for Wellbore Temperature Profile Analysis in Fractured Aquifers

3.1. Heat Fluxes under Ambient and Dynamic Conditions. In hydrogeology, heat fluxes relate to heat advection and heat conduction. Heat advection concerns the flowing and the mixing of groundwater in the aquifer. Heat conduction tends to reequilibrate the temperature of flowing fluids with the temperature of the aquifer and vice versa. T_S and T_D profiles measured in a wellbore are dependent on these two types of heat fluxes, occurring at two scales:

1. Strictly at the borehole scale, heat advection occurs within the water column of the borehole. It is determined by the distribution of groundwater inflows with depth and their respective intensities and temperatures. Free convection due to the variable density of fluids could also drive very slow ambient flows in wells, but this phenomenon is not discussed further in this work. When water flows vertically inside the borehole, its temperature distribution differs from that of T_A. In this case, the vertical temperature profile of the borehole wall is largely controlled by the temperature of the flowing water (T_D). If no flowing water is impacting the wellbore, the temperature of the aquifer surrounding the borehole (T_A) is in equilibrium with the geothermal gradient. If there is a temperature difference between the borehole wall and the aquifer because of flowing fluids, conduction flux occurs between them.

2. Within the portion of the aquifer influenced by the presence of the well or the pumping thereof, heat advection occurs, with groundwater flowing and mixing in fractures, from the furthest extent of the fracture until its interception with the borehole itself. If the orientation of the active fractures is not parallel to the aquifer isotherms (T_A), heat transfer will occur between flowing fluid and the surrounding porous or fractured aquifer. Under such conditions, the temperature of the flowing fluid tends to equilibrate with T_A along its flow paths into the fractured media. Where active fractures intercept the borehole, groundwater finally discharges at a certain temperature (T_i) into the wellbore.

3.1.1. Ambient Water Flows under Static Conditions. In crystalline aquifers, flow patterns are defined by various parameters, such as fracture density, orientation, and hydraulic interconnectivity. In such an environment, and even without artesian conditions, water circulation (i.e., ambient flows) may be induced by the presence of the wellbore itself [40]. The presence of a borehole can actually act as a hydraulic by-pass between fractures that were not connected prior to drilling. For a fractured aquifer without significant porosity, ambient flow inside a borehole has the following main characteristics: (1) it only occurs if two or more hydraulically active discrete fractures or distributed fractured intervals intercept the well, (2) its direction is determined by the head difference between each pair of fractures, (3) its intensity is determined by the combination of hydraulic transmissivity and hydraulic gradients between each pair of fracture zones, (4) it only impacts the length of the interval between hydraulically active fracture(s) that intercept the borehole, (5) its intensity may vary (over the flowing interval) if more than two discrete or distributed fractured intervals are involved, and (6) it can only be unidirectional (the fracture with highest hydraulic head is on one side of the flow interval in the borehole) or bidirectional (discrete or distributed fractures with lower heads are both above and below the fracture with highest hydraulic head).

3.1.2. Water Flow under Pumping Conditions. Under pumping conditions, the discharge of water from the well induces the drawdown of the water column into the borehole. The total resulting drawdown will generally counterbalance ambient flows driven by a small natural head gradient between fractures (e.g., Hess [16] measured ambient flow only as high as 0.3 L/min). When pumping is initiated, all fractures would be drained into the borehole. In this case, groundwater discharge rates into the borehole are essentially proportional to the hydraulic transmissivity of the fractures. If ambient flow has been active in the system for quite a long time, the T_S profile may be significantly different from T_A. When pumping is initiated, T_i would be briefly influenced by ambient T_S rather than T_A profiles. However, as pumping time increases, T_i would be determined by the heat advection of groundwater circulating and mixing in the aquifer (depending on the extension and orientation of fractures) and by the conductive reequilibration of flowing water with the aquifer at T_A.

3.2. Conceptual Example of Temperature Profiles in a Fractured Aquifer. Figure 2 aims to conceptually describe a scenario whereby the hydrogeological context, the bedrock fracture network, and the presence of a well (pumped or not) will drive advection and conduction heat fluxes induced by flowing water. These heat fluxes will modify the temperature field within the system, which could be revealed and described through the measurement of temperatures within the borehole. To simplify, the background geothermal gradient in Figure 2 is considered to be linear; that is, it does not represent a realistic gradient, which is usually multicurved in the upper part, because of seasonal and climatic atmospheric temperature variations [19]. The bedrock aquifer in Figure 2 has three distinct fractures, not connected with one another except at the location of the borehole. These fractures have different inclinations, hydraulic conductivities ($K_2 \gg K_1 \approx K_3$), original temperatures (according to the linear geothermal gradient $T_3 > T_2 > T_1$), and hydraulic heads ($h_1 > h_2 > h_3$) at their furthest extents from the borehole. In this example, heads arbitrarily decrease with depth.

The situation under ambient conditions is presented in Figure 2(a). The highest hydraulic head at the outermost extent of fracture 1 induces an ambient flow that is redistributed between fractures 2 and 3. The flow distribution between the fractures is controlled by the hydraulic potential, which combines the hydraulic transmissivity and the hydraulic gradient between the fractures. In this example, even if $K_2 > K_3$, it is possible that fracture 3 drains a larger proportion of the ambient flow. This can occur if the head gradient between fracture 1 and fracture 3 is high enough that the hydraulic potential is higher than that between fracture 1 and fracture 2. This ambient flow induces a specific temperature profile (T_S) in the wellbore (Figure 2(c)). T_i from fracture 1 is slightly colder than T_A, because the heat advection due to ambient flow along the fracture 1 network is strong enough to avoid its complete reequilibration with T_A. The water flowing upwards then exchanges heat with the borehole walls by heat conduction, implying that the T_S profile differs from the T_A profile. At fracture 2, part of the flow is drained out, so that the total flow within the borehole is reduced, inducing a relatively greater potential for temperature reequilibration by conduction with the borehole wall (increasing the slope of the T_S profile between fracture 2 and fracture 3). Up to fracture 3, T_S is the same as T_A, since no ambient flow influences its profile.

The situation under pumping conditions is presented in Figure 2(b). Due to the pumping, water drawdown into the well imposes the drainage of all active fractures into the wellbore, proportionally to the transmissivity of each fracture. As the pump is placed at the top of the well, flow in the borehole is unidirectional and gradually increases from the lowest to the highest active fracture. Flow intensities during pumping depend on hydraulic properties. However, compared to ambient conditions, flow intensities would be much higher during pumping because active fractures are more strongly solicited and the advection heat flux will become greater than the conduction heat flux. Consequently, the temperature of each inflow discharging into the borehole would be much closer to the temperature of the groundwater

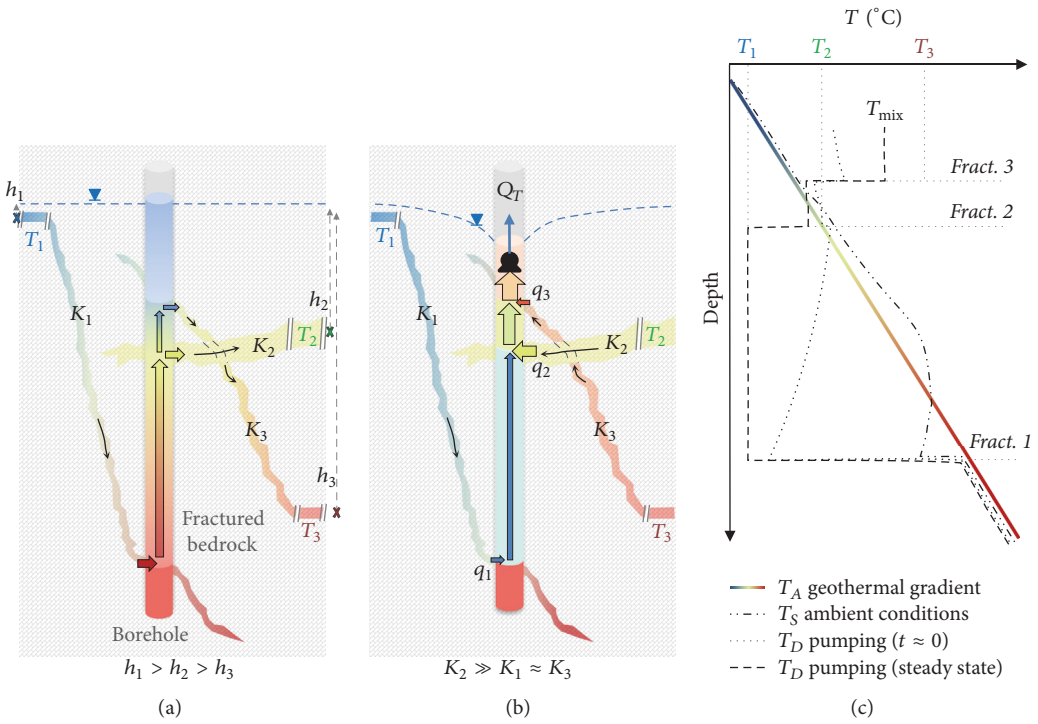

FIGURE 2: Conceptual schematic of temperature profiles in a fractured aquifer: (a) ambient scenario, (b) pumping scenario, and (c) T_S and T_D temperature profiles in the borehole.

at the far end origin of its fracture network. T_i at fracture 1 becomes colder under pumping conditions, because advection dominates over conduction. Once inside the borehole, upward flowing water from fracture 1 would still be subject to conduction-driven reequilibration with the temperature of the borehole wall. However, as its flow rate is much greater during pumping, the relative conductive heat flux is much lower than under ambient conditions. For the short pumping duration ($t \approx 0$) in Figure 2(c), the T_D profile can still slightly reequilibrate with T_S, but as advection will quickly dominate during pumping, the T_D profile is less influenced by conductive reequilibration with the borehole wall. T_D between fractures 2 and 3 is determined by the advective mixing of inflow from fractures 1 and 2 (flow rates and T_i) at the beginning of pumping. With increasing pumping duration, a thermal steady state would eventually be reached (Figure 2(c)). Every T_i will be influenced by the orientation of the fracture system. If the fracture network is inclined, thermal reequilibration within the aquifer could occur, so T_i would range between T_A (at the far end of the fracture network) and T_A (where the facture intercepts the borehole). T_i resulting from very inclined fractures and high flows would be closer to the temperature at the far end of the drainage system. Conversely, if the fracture network is horizontal and flow is weak, T_i would be nearly equal to the temperature imposed by the background geothermal gradient, T_A, at the given depth. When advection controls over conduction (i.e., at steady state in Figure 2(c)): $Ti_{\text{fracture 2}} \approx T_2$, $Ti_{\text{fracture 1}} \gtrapprox T_1$, and $Ti_{\text{fracture 3}} \lessapprox T_3$. The temperature of the total flow discharged at the wellhead (T_{mix} in Figure 2(c)) would mainly be determined by the mixing of inflows from fractures 1, 2, and 3, in proportion to their respective inflow intensities and temperatures.

3.3. Heat Budget at the Borehole Scale. The heat budget at the scale of a given volume (dV) of the borehole is presented in Figure 3. dV is defined by the interval separating two passive temperature measurements, $T(z+1)$ and $T(z-1)$. During pumping, water mixing occurs between groundwater inflow, $q(z)$ (being positive if water enters the borehole and negative if water flows outward) at temperature $T_i(z)$, and water flowing upward ($Q(z-1)$) in the borehole at temperature $T_D(z-1)$. The heat budget of mixing these volumes corresponds to the difference in heat transported by the volume of water entering the base ($Q(z-1)$) and flowing though the wall between $z-1$ and $z+1$ (inflow $q(z)$) and that transported by the water leaving dV at $z+1$ ($q(z)+Q(z-1)$).

For a quantity of water that is either heated or cooled, the general expression of advection heat flux, ϕ_{adv} (W), is given by (2) [41], where Q (m^3/s) is the water flow rate, C ($\text{J m}^{-3\circ}\text{K}^{-1}$) is the specific volumetric thermal capacity of water, and T_i and T_f are the initial and final temperatures of the water, respectively.

$$\phi_{\text{adv}} = QC\left(T_f - T_i\right). \tag{2}$$

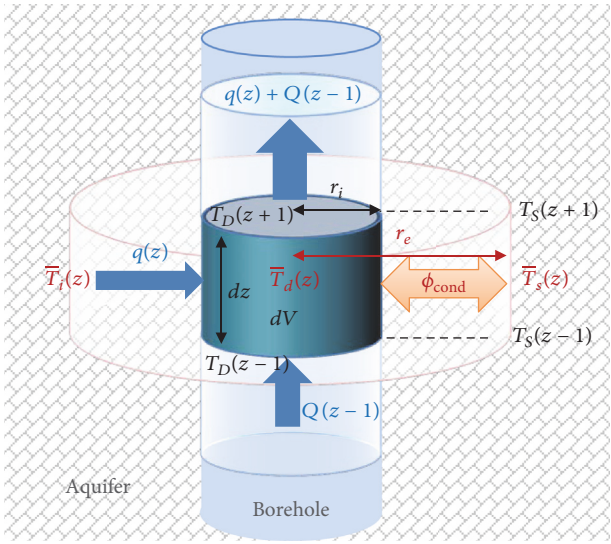

FIGURE 3: Heat budget at the borehole scale.

Considering (2) and the adiabatic mixing of two fluids at different temperatures, the heat balance of water fluxes $q(z)$ and $Q(z-1)$ that mix in the borehole is given by

$$q(z)\,C\left[T_D(z) - \overline{T}_i(z)\right] + Q(z-1)\,C\left[T_D(z+1) - T_D(z-1)\right] = 0. \quad (3)$$

Once pumping is initiated, the borehole wall temperature quickly shifts from T_S to T_D. Heat conduction then occurs radially through the surface of the borehole. The general expression of radial conductive heat transfer at steady state through a semi-infinite solid [41] is applied. In this case, the finite boundary is the borehole wall, which is subject to a temperature shift due to pumping. The temperature anomaly will propagate within the semi-infinite solid (e.g., the aquifer). Heat conduction flux between the borehole wall and the aquifer is then given by (4), where dz is the length of the interval, $\overline{T}_s(z)$ and $\overline{T}_D(z)$ are the mean temperatures of the water in the borehole under static conditions and during pumping respectively, averaged for the interval dz, r_i (m) is the radius of the well, r_e (m) is the time-dependant radius of the heat conduction influence around the borehole, and $x = r_e - r_i$ is the annular distance of propagation of the temperature anomaly due to pumping ($T_D - T_S$), which dissipates into the aquifer. With increasing pumping duration, r_e increases in (5), so that the heat conduction flux fades during pumping. λ (W m^{-1}°K^{-1}) is the bulk thermal conductivity of the aquifer.

$$\phi_{cond} = \frac{2\pi\lambda dz\left[\overline{T}_S(z) - \overline{T}_D(z)\right]}{\ln\left(r_e/r_i\right)}. \quad (4)$$

Considering advection and conduction heat fluxes, the heat balance at the borehole scale is given by (5), which combines (3) and (4):

$$q(z)\,C\left[T_D(z) - \overline{T}_i(z)\right] + Q(z-1)\,C\left[T_D(z+1) - T_D(z-1)\right] = \frac{2\pi\lambda dz\left[\overline{T}_S(z) - \overline{T}_D(z)\right]}{\ln\left(r_e/r_i\right)}. \quad (5)$$

This equation then links the measured temperature-depth profiles (i.e., $T_S(z)$ and $T_D(z)$) with three variables: $q(z)$, $\overline{T}_i(z)$, and r_e (which increases with pumping duration). $q(z)$ distribution could also be measured independently, for example, with a flowmeter.

4. Results

4.1. Depth-Temperature Profiles Modelled with the Heat Budget. In this section, temperature-depth profiles were modelled for dynamic conditions ($T_D(z)$), considering a conceptual well which intercepts six hydraulically active fractures (Figure 4). In this example, the percentage of total pumping discharge (% $Q_T(z)$) and temperature ($\overline{T}_i(z)$) associated with each inflow have been randomly and arbitrarily set with depth. In order to simplify the thermal static conditions, a linear geothermal gradient was applied (arbitrarily set to –1°C/100 m), with an absence of ambient flows so that $T_S(z) = T_A(z)$. Pumping occurs at the top of the wellbore, inducing upward water flows. Blue arrows in Figures 4(b) and 4(c) represent water flow directions in the water column and inflow from the aquifer. The $T_D(z)$ response to pumping was modelled using the heat budget (see (5)) implemented in a spreadsheet, with a vertical resolution $dV = 0.5$ m. Fixed parameters used for the model are as follows: radius of the well, $r_i = 0.075$ m, bulk thermal conductivity of the aquifer, $\lambda, = \lambda_s^{(1-n)}\lambda_w^{\,n} = 1.88$ W m^{-1}°K^{-1}, effective porosity, $n, = 0.05$, and thermal conductivity of sedimentary bedrock, $\lambda_s, = 2.0$ Wm^{-1}°K^{-1} and of water, $\lambda_w, = 0.6$ W m^{-1}°K^{-1} [42]. Various conditions for heat advection and conduction fluxes were simulated to evaluate their effect on the shapes of the $T_D(z)$ profiles. The effect of heat advection (at the given heat conduction, $r_e, = 0.091$ m) was investigated by varying the total pumping rate from $Q_T = 1$ L/min to $Q_T = 100$ L/min (Figure 4(b)), and the effect of heat conduction (at the given heat advection, $Q_T, = 40$ L/min) was investigated by varying r_e from 0.076 to 0.101 m (Figure 4(c)). In both simulations, $T_D(z)$ profiles are also provided by considering only heat advection. Conduction is neglected by setting $\phi_{cond} = 0$ in (5). This is theoretical, because in reality conduction always occurs, but the latter $T_D(z)\phi_{cond} = 0$ profiles are helpful to Figure 4 for visually distinguishing when heat advection becomes dominant over heat conduction.

4.1.1. General Patterns and Processes Controlling Modelled Depth-Temperature Profiles. The positions of water inflows into the wellbore are easily identifiable in the dynamic temperature profiles in Figure 4. However, even if q (5 m) = 20% Q_T and q (20 m) = 10% Q_T (Figures 4(b) and 4(c)), the occurrence of these large inflows is not very well-revealed from the T_D profile, because T_i (5 m) ≈ T_D (5 m) and T_i (20 m) ≈ T_D (20 m). These slight T_D shifts are thus enhanced when

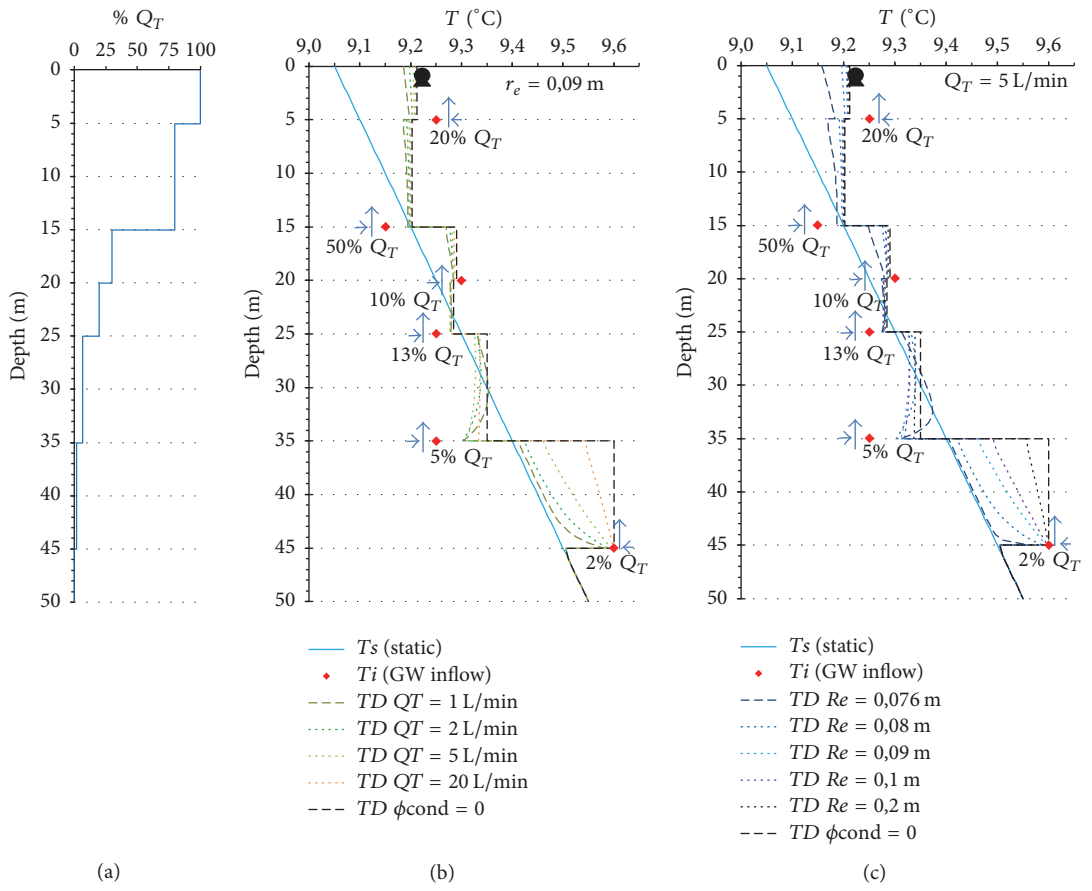

Figure 4: Dynamic depth-temperature profiles modelled with the heat budget.

pumping conditions favor heat conduction (i.e., lower total discharge in Figure 4(b) or lower r_e values in Figure 4(c)).

As T_D profiles are derived from both advection and conduction heat fluxes, the shape of the temperature profiles does not directly (graphically) reflect the water flow distribution in the wellbore. In Figures 4(b) and 4(c), temperature profiles do not mimic the shape of water flow distribution in the wellbore. Even when conduction is neglected ($T_D\phi_{\text{cond.}} = 0$ in Figures 4(b) and 4(c)), the resulting T_D profiles still do not directly reflect water flow distribution in the wellbore. Another important characteristic to note is that when conduction is (or becomes) negligible in this case, $T_D(z)$ profiles are entirely controlled by the distribution of inflows into the wellbore, independently of the total discharge rate.

T_D profiles appear to be extremely sensitive to very low groundwater inflows into the wellbore, especially at the bottom intervals for this example, where the total flow of water remains low. In this example, the bottom inflow, q (45 m), would be detectable for flows as low as 0.02 L/min (e.g., in Figure 4(b), where q (45 m) = 2% of Q_T = 1 L/min, with medium conduction, r_e = 0.091 m) or as low as 0.1 L/min (e.g., in Figure 4(c), where q (45 m) = 2% of Q_T = 5 L/min, with intense conduction, r_e = 0.076 m).

As $T_D(z)$ profiles depend on the temperature of each inflow, the range for each $T_i(z)$ could be qualitatively estimated by visualizing the cooling (e.g., $T_i(z) < T_D(z)$) or warming (e.g., $T_i(z) > T_D(z)$) of the water column where steps in the profile occur.

The influence of heat conduction fluxes could become less important than heat advection with increasing pumping time and/or with increasing water flow rates in the borehole. In Figure 4(b) (representing increasing pumping rates), T_D profiles become dominated by heat advection for Q_T (35 m) > 1.4 L/min (e.g., 7% of Q_T = 20 L/min at depths shallower than 35 m). In Figure 4(c) (representing increasing pumping time; e.g., increasing r_e, with Q_T = 5 L/min), T_D profiles become dominated by heat advection as soon as $r_e > 0.081$ m for Q_T (35 m) > 0.35 L/min (e.g., 7% of Q_T = 5 L/min at depths shallower than 35 m). It is important to note that a radius of influence of r_e = 0.081 m represents a temperature front due to pumping that radially penetrates only 6 mm into the aquifer (r_i = 0.075 m in this case).

Another way to look at the respective influences of advection and conduction fluxes at the borehole scale is given in Figure 5, which provides a comparison of advection and conduction fluxes calculated at the borehole scale using (2) and (4). Advection heat flux in the wellbore is related to flow and to the cooling or warming of the water (ΔT) due to inflowing groundwater. Conduction heat flux between the borehole wall (at T_D) and the aquifer (at $T_S = T_A$) varies logarithmically with the propagation distance ($x = r_e - r_i$) of the temperature offset ($T_D - T_S$) into the aquifer.

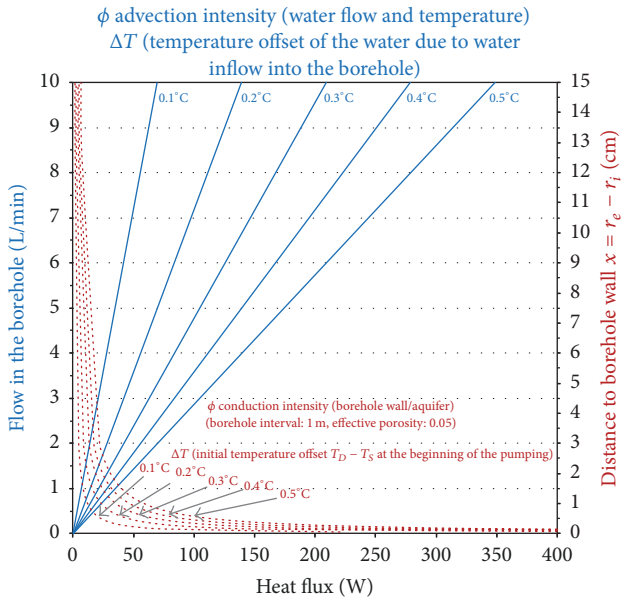

FIGURE 5: Comparison of advection and conduction heat fluxes at the borehole scale. $\Phi_{advection} = f$ (total flow rate, temperature offset due to groundwater inflow) and $\Phi_{conduction} = f$ (distance of radial temperature propagation into the aquifer, $T_D - T_S$ offset).

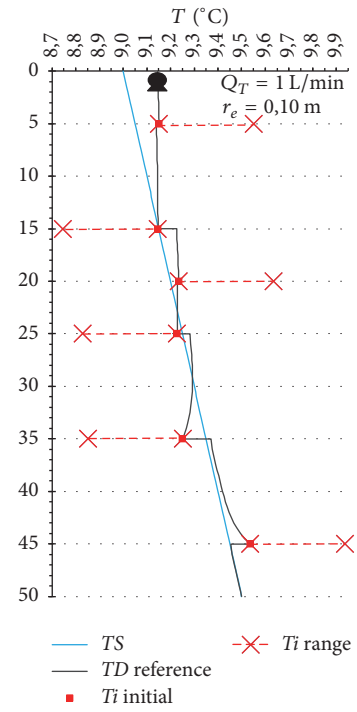

FIGURE 6: Example of $T_i(z)$ initialization prior to $T_D(z)$ modelling with the heat budget.

Conduction flux is therefore intense at the beginning of the pumping ($r_e \approx r_i$) and fades with pumping duration (i.e., with increasing r_e). Interpretation of Figure 5 indicates that conduction flux is higher than advection flux when flow rates are less than 1 L/min and when temperature propagation is less than approximately 1.5 cm into the aquifer ($r_e = 0.09$ m; $r_i = 0.075$ m). Conversely, if water flow is greater than 1 L/min in the borehole, with increasing pumping duration (i.e., $x >$ 1.5 cm), advection fluxes become higher than conduction.

4.1.2. Potential of a High-Resolution Temperature Probe to Be Used as a Flowmeter. A relevant question is whether passive temperature measurements could directly reflect the water flow distribution in the wellbore. This question is investigated in this section by modelling depth-temperature dynamic profiles with the heat budget, with $T_i(z)$, $q_i(z)$, and r_e as variables. The fitting procedure consists of minimizing the root mean square error (RMSE) of T_D (see (6)), where $T_{D\text{reference}}(z)$ represents the observed temperature-depth profiles, $T_{D\text{model}}(z)$ represents the modelled temperature-depth profiles, D_{total} is the total depth of the wellbore, and dz is the vertical resolution of the heat budget. D_{total}/dz represents the number of $T_{D\text{model}}(z)$ calculated with the heat budget.

$$\text{RMSE } T_D = \sqrt{\frac{\sum \left(T_{D\text{model}}(z) - T_{D\text{reference}}(z)\right)^2}{D_{\text{total}}/dz}}. \quad (6)$$

In this example, the fitting procedure has 13 variables ($6T_i(z)$, $6q_i(z)$, and r_e) and is constrained by $100T_D(z)$ observations (well depth of 50 m, with a vertical resolution of $dz = 0.5$ m). To avoid divergence of the iterative procedure, $T_i(z)$ variables were initialized and constrained for each water inflow. Inflow temperatures $T_i(z)$ were initialized at $T_{D\text{reference}}(z)$ (T_{initial} in Figure 6) and constrained within the range of $T_i(z) = T_{D\text{reference}}(z) \pm \Delta T$ (T_{irange} in Figure 6). The temperature range is logically anchored depending on the cooling or warming of the T_D profile resulting from inflows. For the situation wherein the water column is cooling (because of cold inflow), the range is set to $T_{D\text{reference}}(z) - \Delta T < T_{\text{irange}} < T_{D\text{reference}}(z)$ and vice versa for a warming situation ($T_{D\text{reference}}(z) < T_{\text{irange}} < T_{D\text{reference}}(z) + \Delta T$). In this example, ΔT was arbitrarily set to 0.4°C, but a large possible range over which $T_i(z)$ may vary is permitted before the fitting procedure converges. Water inflow intensities were all initialized at very low flows ($q_i(z) = 0.0001$ L/min) and constrained so that the total modelled discharge must be equal to the total reference discharge. Finally, conduction in the borehole is initialized as being intense ($r_e = 0.076$ m) and constrained within the possible range (i.e., $r_e > r_i$).

For modelling, two reference $T_{D\text{reference}}$ profiles were generated using the conceptual model (as described at the beginning of Section 4.1), with conduction set to $r_e = 0.10$ m and total pumping rates of 1 L/min (Figure 7) and 20 L/min (Figure 8).

The fitting procedure very efficiently models $T_D(z)$ in both cases. As shown in Figures 7 and 8, $T_{D\text{reference}}$ and $T_{D\text{model}}$ appear graphically superimposed. Numerically, some discrepancies remain, but the RMSE remains low in both cases (RMSE $T_D \approx 10^{-4}$). The fitting procedure adequately models the whole system at a low discharge rate ($Q_T = 1$ L/min, Figure 7), associated with low error for each variable; $T_i(z)$ (RMSE $T_i = 1.2 \times 10^{-5}$°C), $q_i(z)$ (RMSE $q_i = 1.8 \times 10^{-3}$ L/min), and $\Delta r_e = 8.7 \times 10^{-4}$ m ($\Delta r_e = r_{e\text{model}} - r_{e\text{reference}}$). At a higher

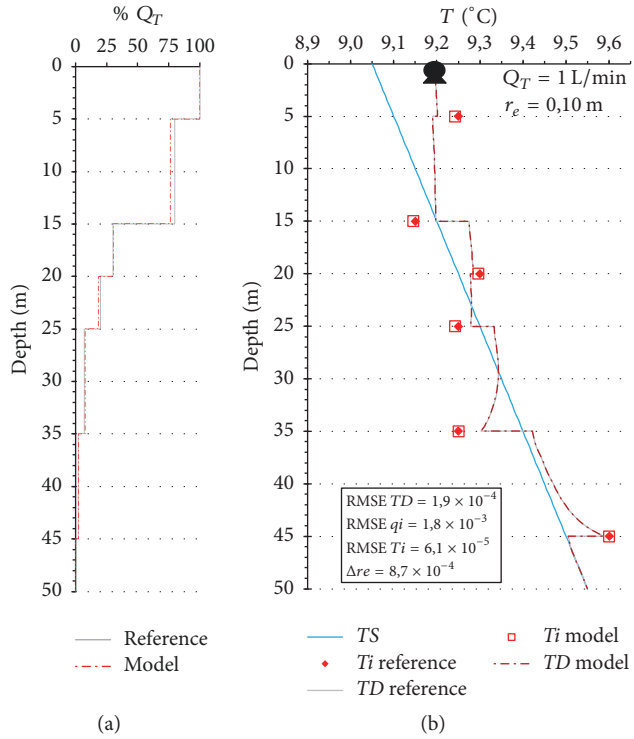

FIGURE 7: Results of $T_D(z)$ modelling with the heat budget at $Q_T = 1$ L/min. (a) Flow-depth distribution; (b) dynamic temperature profiles ($T_D(z)$) and temperatures of inflows ($T_i(z)$).

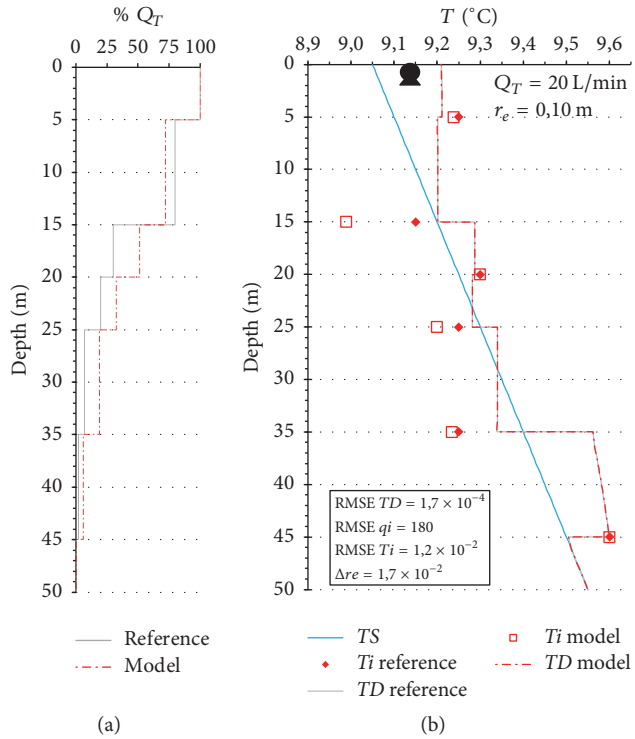

FIGURE 8: Results of $T_D(z)$ modelling with the heat budget at $Q_T = 20$ L/min. (a) Flow-depth distribution; (b) dynamic temperature profiles ($T_D(z)$) and temperatures of inflows ($T_i(z)$).

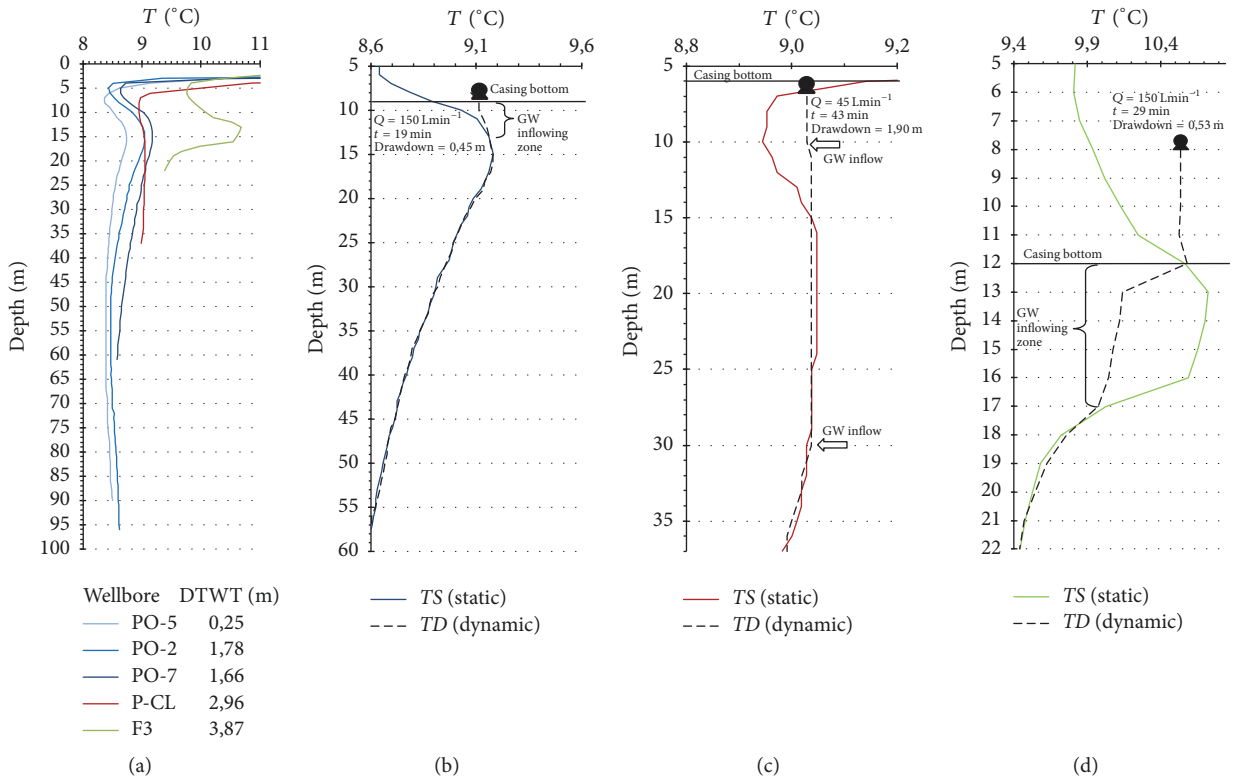

FIGURE 9: Temperature profiles in June 2016 for all wells under static conditions (a) and under static and dynamic conditions for wells PO-7 (b), P-Cl (c), and F3 (d).

discharge rate (Q_T = 20 L/min, Figure 8), errors for modelled variables increase, with RMSE $T_i = 1.2 \times 10^{-2}$°C, RMSE q_i = 180 L/min, and $\Delta r_e = 1.7 \times 10^{-2}$ m. The ability of the model to converge to accurate variable values depends on the degree of curving for the $T_D(z)$ profiles. The more the profile is curved along the entire profile due to the dominant influence of conduction over advection, the easier the fitting procedure can converge within a narrow, accurate range for the variables T_i, qi, and r_e. Even a very slight influence of conduction would theoretically induce a slight curvature in $T_D(z)$, so that the model can theoretically always be solved. However, with the diminishing influence of conduction, the preciseness (and complexity) of the fitting procedure has to proportionally increase to still obtain the narrowest and most accurate range of solutions for the variables. At the other extreme, if there is no conduction at all, the model can still perfectly converge to fit the $T_D(z)$ profiles, but an infinity of solutions is possible for each pair of $T_i(z)$ and $q_i(z)$ associated with the inflows. This is because, without conduction, any variation in $T_i(z)$ could be numerically compensated by $q(z)$ to give the same perfectly square $T_D(z)$ profiles that are observed after mixing.

4.2. Field Applications

4.2.1. Qualitative Interpretation of Field Depth-Temperature Profiles. PO-2, PO-5, and PO-7 temperature logs under static conditions (Figure 9(a)) were taken on the same day and represent typical static temperature profiles not influenced by ambient flows. Heat pulse flowmeter tests [43] were performed for well PO-7 under static conditions and did not allow the detection of water circulation in the borehole (the minimum velocity resolution of the device is 0.113 L/min). As PO-2, PO-5, and PO-7 temperature profiles have the same symmetrical curving, it is inferred that ambient flows are so low, if there are any at all, that they do not significantly impact the temperature profiles of these three wells. The corresponding $\mathbf{T_S}$ profiles of the three wells differ by 0.1–0.5°C, which may be explained by different local recharge rates, the nature and thickness of the unconsolidated sediments, or differences in land cover. These discrepancies are not considered further in this work, which focuses rather on borehole logging to characterize active hydraulic fractures. $\mathbf{T_s}$ profiles for wells PO-2, PO-5, and PO-7 are therefore considered to be representative of typical $\mathbf{T_A}$ profiles of southern Quebec: (1) the seasonal variation in soil temperature (from the atmospheric signal) propagates from the land surface down to 15 m depth. The minimum temperature, near 5 m depth, corresponds to the cold temperature signal of winter 2015-2016, which has propagated into the subsurface; (2) from 15 m to 50–60 m, temperatures decrease with depth. This inverse gradient can be explained by the climatic warming in Canada over the last 150–200 years [44]; and (3) deeper than 50–60 m, which corresponds to the transition zone to the normal geothermal gradient, temperatures increase with depth.

Static and dynamic temperature logs of the three pumped wells are superimposed in Figure 9. The PO-7 temperature

log under dynamic conditions (Figure 9(b)) was taken after 19 min of pumping with a discharge rate of 150 L/min. Static and dynamic temperature profiles differ near the surface, down to 13 m depth, and are nearly identical below this depth (i.e., $T_S = T_D$). This indicates that the productivity of this 52 m screened well essentially originates from an only 4 m-long productive interval in the upper part of the well.

For well P-Cl, the static temperature log (Figure 9(a)) already suggests the presence of ambient flow between 15 and 30 m, because the constant temperature within this interval differs from the expected curved T_A profile. Although the direction and intensity of ambient flows could not be determined at this stage, the T_S profile already reveals that an ambient flow of water at 9.04°C is circulating between one or more fractured intervals located in the 15–30 m depth range. The P-Cl dynamic T_D profile, taken after 40 min of pumping with a discharge rate of 45 L/min, confirms the information revealed by the T_S profile but also indicates that the main productive zone must be located near 30 m depth, because its inflow temperature (9.04°C) completely resets the temperature of the water circulating upward along the entire length of the borehole. Other small water inflows from 10 m to 30 m depth may be possible, but as no temperature variation is distinguishable in this interval, the main inflow must be located at approximately 30 m depth.

The T_S profile for well F3 (Figure 9(d)) also suggests the presence of ambient flows, because between 12 and 17 m the profile is overcurved compared to what would be expected from the influence of T_A alone. This suggests that more than two active fracture zones are likely located within the interval between 12 and 17 m, thus creating a complicated temperature pattern. Ambient flows between these active fractures create this anomalous temperature interval. In F3, the T_D profile (Figure 9(d)) was taken after 29 min of pumping with a discharge rate of 150 L/min. As T_S and T_D coincide below 17 m, no active fracture is expected to be present below this depth. Joint analysis of passive and dynamic logs qualitatively reveals the following: (1) the first active fracture zone is located between 16 and 17 m depth and initiates water flow into the borehole, with a bottom inflow temperature of 10.00°C; (2) between 16 and 13 m depth, one single qualitative interpretation is not possible. The temperature gradient retains the same orientation and intensity between each measurement. This could either indicate that warmer water is inflowing ($T_i > T_D$) or that temperature reequilibration by conduction occurs between the borehole and a warmer aquifer neighboring the borehole ($T_S > T_D$) or a combination of these two scenarios. And, finally, (3) between 12 and 13 m, the slope of the dynamic log increases strongly, which can only be explained by warmer water inflow ($T_i > T_D$), which increases substantially.

4.2.2. Quantitative Borehole Investigation: Temperature Logging, Flow Metering, and Televiewing. Flowmeter logging in boreholes PO-7 and F3 was performed with pumping rates as high as possible, depending on the productivity of the given well, in order to maximize water velocities in the boreholes. Different pumping rates were tested on each of the wells (results not shown in this article), with no measurable variation in well inflow distribution found to result with depth. The PO-7 televiewing results are presented in Figures 10(a) and 10(b), and the flowmeter log is presented in Figure 10(c). The flowmeter log revealed that 10% of total inflows originate from a low-fractured interval, located between 12 and 13 m. A discrete fracture is visible at 10.5 m and alone accounts for 74% of the total productivity of the well. The remaining 16% of the inflow originates from a joint or fracture located at 9.6 m depth and from other small fractures located above this and down to the base of the casing. For well F3 (televiewing in Figures 11(a) and 11(b); flowmeter log in Figure 11(c)), small conduits are identifiable through televiewing at 16.5 m depth. Flowmeter measurements show that these conduits account for approximately 7% of the total well productivity. No other water inflow is identifiable through the flowmeter results until above 14 m depth. Televiewing also revealed information about the thickness of strongly fractured banks that alternate with unfractured dolomite intervals. Based on flowmeter results where flow increases, fractured zones from 14 to 13.7 m, 13.4 to 12.8 m, and 12.6 to 12.3 m account for approximately 3, 31, and 46% of the total transmissivity of well F3, respectively. The remaining 13% of the transmissivity likely originates from fractures located near the base of the casing. For wells PO-7 and F3, the distribution of hydraulic conductivities for each productive fractured interval are given in Figures 10(d) and 11(d), respectively, and have been calculated using (1). It should be noted that the spinner flowmeter provided highly valuable hydrogeological information here, with a high vertical resolution (5 cm in this work), and was obtained relatively quickly (i.e., less than half an hour to log a 60 m deep well).

Temperature logs under static and dynamic conditions are presented in Figures 10(e) and 11(e) for wells PO-7 and F3, with close-ups of depth intervals where water inflow occurs and influences $T_D(z)$ profiles. The full-depth scale temperature logs are presented in Figure 9. The heat budget (see (5)) was partially used in this applied case, because the measurement resolution ($dz = 1$ m) for the available data is insufficient to perform the full fitting procedure presented in Section 4.1.2. Also, at the time of measurement, high discharge rates were set to maximize the sensitivity of the flowmeter, while the thermal fitting procedure would instead require low discharge rates to favor conduction (Section 4.1.2). Nevertheless, the heat budget was applied for wellbore PO-7, to calculate mean inflow temperatures (Figure 10(e)), with flow distribution intervals known from flow metering. Given high flow rates and pumping times, conduction was set to low intensity ($r_e = 1$ m). For PO-7, calculated $T_i(z)$ were all warmer than $T_S(z)$ at a 13 m depth, indicating that pumping-induced drainage might all originate from very surficial and warmer horizons, above 5 m depth ($T_S(z)$ profile in Figure 9(a)), influenced by the previous summer's signal propagation within the subsurface. For well F3, $T_i(z)$ can be calculated for very high inflow intervals (12 to 13 m, 13 to 14 m, and 16 to 17 m), with respective $q_i(z)$ measured with the flowmeter (model 1 in Figure 11(e)). For two other intervals (14 to 15 m and 15 to 16 m), flow metering did not reveal any increase in flow, resulting in the nondetection of inflows

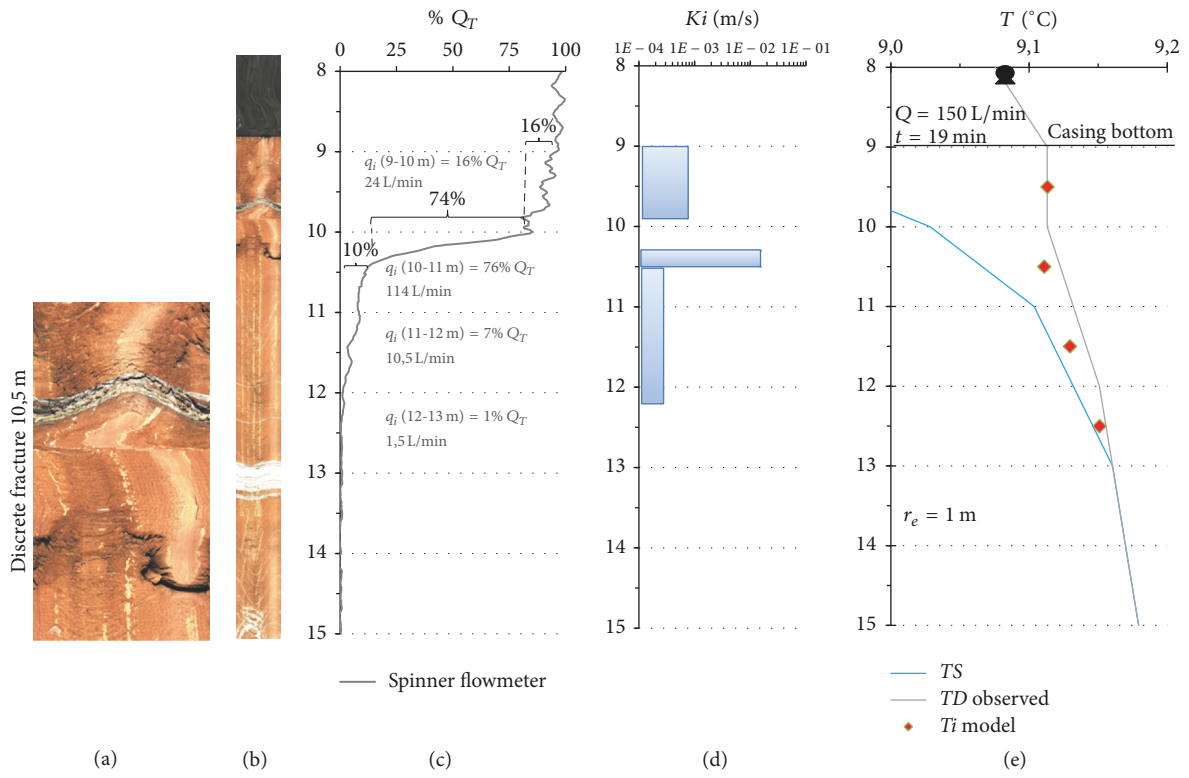

FIGURE 10: Borehole PO-7 logging results: (a) televiewing close-up of the most productive fracture, (b) televiewing log, (c) flow distribution obtained by flowmeter, (d) vertical distribution of hydraulic conductivities obtained by flowmeter, and (e) temperature profiles under static and dynamic conditions and temperature of groundwater inflows calculated with the heat budget.

within these intervals. However, $T_D(z)$ profiles between 14 and 16 m show significant temperature increases. As total advection flow in the water column is already high above 16 m depth (10.5 L/min), increasing temperature between 16 and 14 m cannot be explained by conduction reequilibration towards $T_S(z)$. Examples are given in Figure 11(e) (model 1), representing modelled $T_D(z)$ for various conduction intensities, but with no inflows between 14 and 16 m depth. In this case, $T_D(z)$ modelled between 14 and 16 m could not fit the observed $T_D(z)$ at any conduction intensity without introducing inflows at this interval. The heat budget fitting procedure was then applied to all intervals, including inflows to the 14 to 15 m and 15 to 16 m intervals (model 2 in Figure 11(e)). Conduction intensity in the latter model (2) was arbitrarily set to r_e = 1 m, a value that lowers the influence of conduction, given that the pumping time of the experiment is 29 min. With model 2 (Figure 11(e)), warm inflows, T_i (14-15 m) = 10.70°C and T_i (16-17 m) = 10.51°C, were estimated, corresponding with q (14-15 m) = 0.69 L/min and q (15-16 m) = 0.75 L/min. These calculated values are not very accurate, because the fitting procedure is poorly constrained, with a limited temperature observation (resolution of only dz = 1 m). In this case, warmer $T_i(z)$ could lead to even lower $q_i(z)$ while still perfectly fitting $T_D(z)$. Nevertheless, the most relevant information here is that the combination of temperature measurements (even at a resolution of 0.01°C) and heat budget analysis allows the occurrence of very low inflows to be inferred among the much higher productive intervals characterizing wellbore F3. Discussion linking the $T_i(z)$ values of well F3 to the depth at which groundwater is drained during pumping is provided in Section 4.2.3 through more detailed experiments and analysis.

4.2.3. Inference of Groundwater Origin from Transient Temperature Logging and Heat Budget Application. Two temperature logs were obtained for well F3, in June and November 2016. In Figure 12(a), T_s measured in June 2016 showed a colder water interval from 5 to 11 m depth (influenced by cold air temperature at the ground surface for winter 2015-2016), followed by a warmer zone from 11 to 17 m (influenced by warm air temperature at the ground surface for summer 2015). T_s measured in November 2016 showed the influence of summer 2016 from the top of the water table until 12 to 13 m depth and likely a smoothed downward propagation of the summer 2015 signal below 17 m. Figures 12(b) and 12(c) present T_s and T_D for June and November 2016, respectively, along with T_i for each pumping time and discharge rate. T_i values were calculated using the heat budget at the borehole scale (see (5)) for the most productive intervals identified by flow metering (Section 4.2.2) to be 70, 23, and 7% of the total transmissivity of well F3 for the 12 to 13 m, 13 to 14 m, and 16 to 17 m depth intervals, respectively.

For both June and November logs, T_i profiles already differ from T_s shortly after the beginning of pumping. These

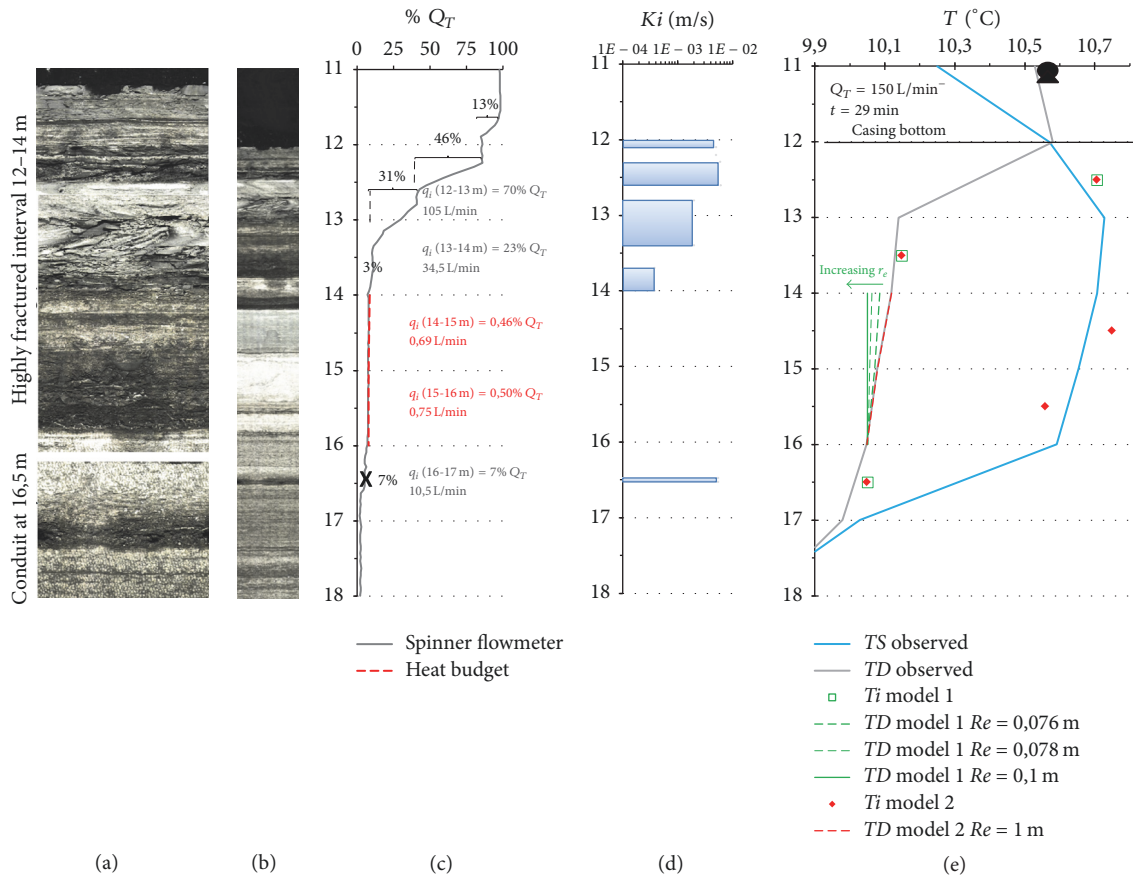

FIGURE 11: Borehole F3 logging results: (a) televiewing close-up of productive intervals, (b) televiewing log, (c) flow distribution obtained by flowmeter and flow calculated with the heat budget between 14 and 16 m depth, (d) vertical distribution of hydraulic conductivities obtained by flowmeter, and (e) temperature profiles under static and dynamic conditions and temperature of groundwater inflows calculated with the heat budget.

discrepancies suggest that, soon after pumping began, T_i patterns are influenced by inflows originating from active fracture networks in equilibrium with T_A. This also indicates that ambient flows (between 12 and 17 m depth) imposing the T_S profiles around the borehole mask the T_A profile. T_i temperatures then appear to be very rapidly controlled by the temperatures within drained horizons, the temperatures of which depend on the seasonal T_A signal. In June (Figure 12(b)), T_i is warmest in the 12 to 13 m interval and must drain the warmer horizon influenced by summer 2015 (13 to 16 m depth), because temperatures for over- and underlying intervals are colder. T_i for the two lower inflow intervals (13 to 14 and 16 to 17 m depth) are colder and, with respect to the T_S profiles for June, could drain colder horizons either above 11 m depth or below 17 m depth. However, analysis together with the November profiles (Figure 12(c)) shows that T_i from 13 to 14 and 16 to 17 m depth must drain cold water originating from below 17 m, because intervals above 11 m depth are warmer and cannot explain such cold temperatures. Although the interpretation of temperature inflow patterns in Figures 12(b) and 12(c) remains difficult, one key piece of information provided is that all T_i values become cooler as pumping duration increases, independently of the season. This suggests that cold water originates from horizons deeper than 17 m depth.

The evolution of inflow temperatures, $T_i(z)$, in well F3 during pumping in November is presented in Figure 13. The temperature range from the beginning to the end of pumping is comparable for every depth interval. This common cooling of all inflows with time suggests that all inflows drain stratified fractured horizons and have comparable orientations. It can be noted that, even after 150 min of pumping at high discharge rates (150 L/min at the final stage), none of the inflow temperatures reaches a plateau. This means that temperature equilibration by conduction between flowing groundwater and the aquifer has not yet reached a thermal steady state along the flow path from the origin of aquifer drainage to the wellbore. Even if it is not quantified here, this suggests rather long conduits or channelized flow paths. In such a case, the reequilibration of the water temperature by heat conduction would take longer, because surface exchange with the aquifer is low. Conversely, thermal conduction equilibration occurring in a highly homogeneously fractured aquifer (or even a porous medium) would reach a steady state much faster, as the water/aquifer surface exchange is much higher. Compared to the two other fractured intervals,

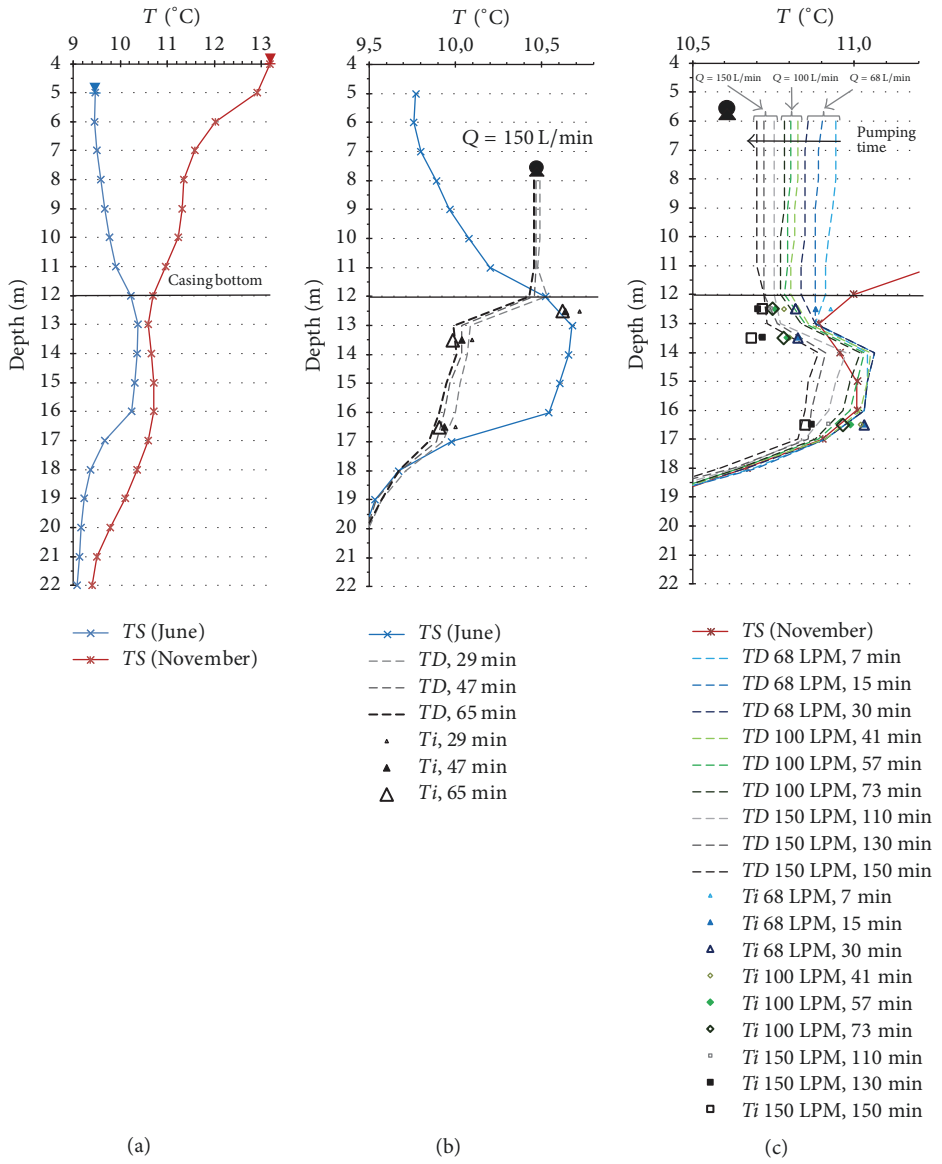

Figure 12: Temperature profiles in well F3: static conditions for June and November 2016 (a); static and dynamic conditions with several discharge rates and pumping durations for June (b) and November (c). T_i are the mean inflow temperatures calculated using the borehole-scale heat budget.

the increasing cooling rate of the lower interval (16 to 17 m depth) appears to coincide slightly better with the increase in pumping rate. Such a proportional thermal response may also indicate that the bottom inflow (16.5 m depth) would be the most channelized of all inflows, responding faster to advection changes, because of the lesser influence of conduction.

5. Discussion

5.1. Qualitative Interpretation of Depth-Temperature Profiles

5.1.1. Utility of Temperature Profiles to Infer the Occurrence and Position of Water Inflows into the Wellbore. Under static conditions, temperature profiles are rather complex close to the surface. In the typical Quebec context shown in Figure 9(a), T_A profiles are characterized by two inflexion points, and temperature in the top 15 m varies quite substantially and rapidly with the seasons. However, ambient water flows into the borehole may be detected using passive temperature logging by the interruption of the smoothed shape of these profiles. Temperature logs for the three wells studied here under static conditions allowed the presence or absence of ambient water circulation in the borehole to be inferred and if detected (for wells P-Cl and F3), allowed the intervals where active fractures are present to be rapidly determined. In general, if two or more hydraulically active fractures intercept a borehole at different depths, even a small hydraulic gradient between them would induce ambient flows into

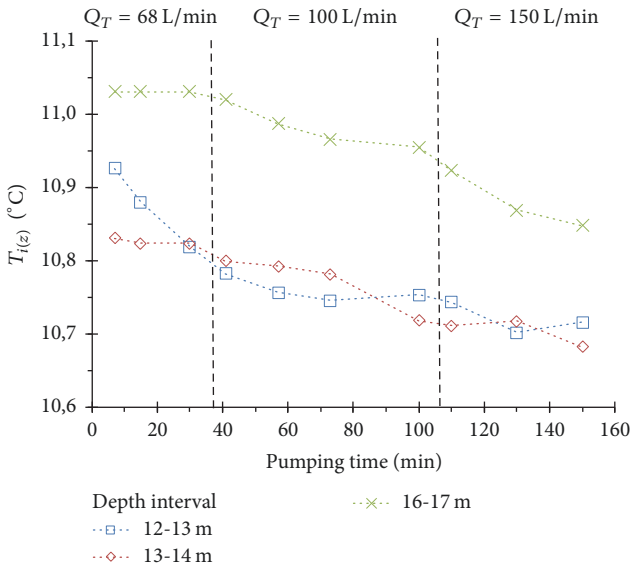

Figure 13: Evolution of main inflow temperatures ($T_i(z)$) in well F3 during November 2016 pumping.

the borehole. As even small ambient flows are detectable by anomalous temperatures, logging under static conditions is a very efficient technique with which to identify productive fractured intervals in boreholes. Even if fractured zones are only identified qualitatively with static temperature logs, this remains very efficient, because the information on productive intervals could only otherwise be obtained by using more costly or sophisticated measurements (e.g., flow metering, packer testing, and tracers).

Under pumping conditions, temperature logging allows information obtained under static conditions to be either reinforced or clarified. Dynamic temperature profiling presents a portrait of water inflow solicited from hydraulically active fractures by pumping. In general, as shown theoretically in Figure 4 and in applied cases in Figure 9, the position of water inflows due to pumping should be easily identifiable in a first reading of high-resolution temperature profiles. However, if the temperature of a water inflow is very similar to the temperature of water flowing in the wellbore, the occurrence of the inflow cannot easily be detected by a single temperature log, even if the inflow intensity is high. Nevertheless, even a slight temperature shift would still be detectable through the use of high-resolution temperature probes (0.001°C). Such a high sensitivity may be further enhanced with the implementation of pumping procedures that favor heat conduction (i.e., low total discharge, temperature logging from the beginning of pumping). Theoretical examples of this are given in Figure 4 for inflows at 5 and 20 m depths, and applied examples for well F3 are given in Figure 11, where interpretation of T_D profiles between 14 and 16 m suggests the occurrence of very low inflows, which are not detectable by flow metering.

5.1.2. Utility of Temperature Logging to Reveal the Occurrence of Low Flows in the Wellbore. High-resolution temperature profiling appears to be extremely sensitive and to reveal very low groundwater inflows into boreholes. Even low pumping flow rates present a great advection potential, such that even a slight change in inflow temperature with pumping time would induce a detectable variation in the slope of the temperature profile, thus making low rates of inflow detectable. Such sensitive detection could even be applied to the low flows associated with the lowest productivity zone in a well during pumping (theoretical example in Figure 4 and applied examples in Figures 9, 10, and 11). However, in such cases, the detection of low inflows is enhanced within intervals of the borehole where the total flow of water remains low. If the pump is placed at the top of the borehole, the location of the lowermost active fracture could be more clearly defined, because it is located at the beginning of the divergence between static and dynamic temperature logs. However, the position of the pump can be adapted to allow low flow detection for different inflow distributions with the depth. If the pump is placed at the top of the well, small inflows located in the lower part of the borehole become much harder to detect if high inflow is present higher in the borehole. This issue could be addressed by performing two pumping tests, one with the pump placed at the bottom of the borehole and one with the pump placed at the top of the borehole. As mentioned in the previous paragraph, low flow, ultimately associated with only a slight T_D shift, should become visible even at low pumping rates by using a temperature sensor that has a high enough resolution, or by adapting pumping conditions so as to reveal them. The high sensitivity of temperature to low flows is of particular interest to reveal ambient (very low) flows when they occur in wells (i.e., Figures 9(c) and 9(d)). Ambient flows are usually not easily detectable without sophisticated instrumentation and delicate device operation, for instance, in the case of heat pulse flow meters.

5.1.3. Interpretability of Temperature Profiles against Water Flow Distributions in the Wellbore. Inferring flow distribution from temperature profiles is not straightforward. Processes that shape temperature profiles are complex, and temperature profiles will therefore not directly (graphically) reflect the water flow distribution in the wellbore. In the context of fractured aquifers, fractures can be oriented in a complex manner, so that the temperature of water discharging into the borehole can be quite randomly distributed with depth. None of the theoretical (Figure 4) or applied (Figures 9, 10, and 11) examples allows the water flow distribution in the wellbore to be directly inferred just from a simple reading of passive temperature logs. Temperature profiles do not mimic the water flow distribution in the wellbore, because implied heat fluxes are defined by both heat advection and conduction fluxes. Even when heat advection dominates over heat conduction ($\phi_{\text{adv.}} \gg \phi_{\text{cond.}}$), heat advection fluxes rely on both flow intensity and the associated temperature (see (2)), so that the resulting temperature profiles will not directly reflect the water flow distribution in the wellbore. Therefore, without using a heat budget, the interpretation of temperature profiles does not allow inflow intensities into the wellbore to be quantified.

5.1.4. Inferring the Temperature Range of Water Flowing into the Wellbore. As depth-temperature profile shifts depend on the temperature of inflows, the temperature range for each inflow could at least be estimated by visualizing the cooling (e.g., $T_i(z) < T_D(z)$) or the warming (e.g., $T_i(z) > T_D(z)$) of the water column where steps are seen in the profile. An example of a theoretical T_i range is given in Figure 6, which served to initiate $T_D(z)$ modelling in Section 4.1.2. This logical interpretation provides a valid range in applied cases (Figures 9, 10, and 11), without performing a heat budget calculation.

5.2. Potential of and Limitations to Quantitative Interpretation Using the Heat Budget at the Borehole Scale. Numerical models are able to assess the thermal response of hydrogeological systems extremely well [31]. However, these sophisticated models are generally very time-consuming to generate. At the borehole scale, the use of an analytical heat budget may complement numerical modelling or could even represent a very good and fast alternative for different types of quantitative investigation, as discussed below.

5.2.1. Temperature Probes to Infer the Origin of Groundwater Drained from the Aquifer. If a wellbore is logged for both passive high-resolution temperature and flow metering, the temperature of inflows can easily be calculated using the heat budget (Section 3.3). The determination of the inflow temperatures during pumping provides precious information regarding the origin of the groundwater drained from the fractured aquifer. Inflow temperatures are controlled by heat conduction occurring between groundwater flowing along flows paths and the aquifer neighboring the water-channeling fractures. Except for large conduits, such as in karsts, flow velocities and fracture apertures are generally rather small, such that the large specific surface allows for large conductive fluxes. As water flow converges towards a well, advection fluxes become denser. This implies that, with increasing distance from the well, conductive heat flux between the aquifer and flowing water would eventually dominate over heat advection, while, closer to the well, advection should eventually dominate over conduction. Therefore, with increasing distance from the well, the temperature of circulating water tends to be in equilibrium with T_A. With sufficient pumping duration and intensity, the temperature of water discharging into the borehole (T_i) will approach the temperature in the region of the aquifer where water enters the fractured network (T_A). If fractures are discrete conduits, the extent from their origin to the borehole may represent relatively long distances. However, if a fracture network is distributed, with small apertures, its thermal advection and conduction behaviour would be equivalent to a porous medium. In this latter case, it is inferred that T_i would be in equilibrium with T_A within few meters of the borehole.

5.2.2. Potential of Temperature Probes as Integrated Quantitative Tools for Wellbore Investigation. The simultaneous use of temperature measurements and heat budget fitting procedures may, in certain conditions, provide quantitative information about both the temperature and the intensity of inflows. Theoretical examples presented in this work (Section 4.1.2) suggest that if highly curved depth-temperature dynamic profiles are obtained, a fitting procedure using the heat budget would be capable of quantifying both temperature and intensity of inflows. From a measurement perspective, the success of such a fitting procedure is dependent on the resolution the temperature probe (°C) and on the vertical interval (dz) between temperature measurements. For fractured aquifers, the number and the distribution of temperature measurements must exceed those of the hydraulically active fractures. Only a few fractures would be adequately constrained by just a few temperature measurements, whereas if numerous fractures are involved, the number of temperature measurements required would consequently increase. From a field work perspective, such temperature modelling would more successfully characterize wellbores presenting discrete active fractures, or active fractured intervals that are at least clearly separated by nonproductive intervals. In these contexts, low discharge pumping rates should be preferred over high rates, in order to favor curved depth-temperature profiles. It is, however, assumed that, in many applied cases, the complexity of inflow distribution in wellbores would not allow a complete inflow characterization with only high-resolution temperature measurements and a heat budget. Nevertheless, even in such cases, the use of passive temperature logging and a heat budget would still be highly complementary to flow metering for characterizing very low inflows that would not otherwise be detected, or to calculate the temperature of inflows.

6. Conclusions

A difficult and often incompletely resolved task for hydrogeologists is to assess the origin and directions of groundwater flow paths in heterogeneous media. Far from being systematically used, some borehole logging techniques allow the distribution of aquifer hydraulic properties to be described with depth. High-resolution temperature logging has great potential to contribute to such assessments. In some cases, the temperature probe could act as a very sensitive flowmeter in fractured aquifers. Temperature logging is done very quickly, and temperature profiles efficiently identify productive sections in boreholes, so as to infer where they originate from within the aquifer. With measurements made under pumping conditions, and using some simple analytical heat budgets, temperature logs are among the rare techniques that permit inference on the origin of groundwater that is drained into the borehole. Furthermore, this information is collected without injecting and/or monitoring any anthropogenic tracer into the aquifer. Data acquired from temperature logging concurrent with other borehole logging techniques remains of great interest for improving the quality of hydrogeological applications. Such information would help to constrain flow and transport numerical models during both their construction and their calibration, to then delineate wellhead protection areas, identify subsurface flow paths of contaminated sites, and inform other water management issues where vertical aquifer stratification needs to be considered, in terms of both hydrogeochemistry and groundwater age distribution.

Conflicts of Interest

The authors declare that there are no conflicts of interest regarding the publication of this paper.

Acknowledgments

This research was supported by the Natural Sciences and Engineering Research Council of Canada (NSERC), in partnership with Envir'Eau-Puits Inc., which also kindly provided access to the experimental sites.

References

[1] G. De Marsily, F. Delay, J. Gonçalvès, P. Renard, V. Teles, and S. Violette, "Dealing with spatial heterogeneity," *Hydrogeology Journal*, vol. 13, no. 1, pp. 161–183, 2005.

[2] D. Schulze-Makuch, D. A. Carlson, D. S. Cherkauer, and P. Malik, "Scale dependency of hydraulic conductivity in heterogeneous media," *Groundwater*, vol. 37, no. 6, pp. 904–919, 1999.

[3] R. Raghavan, "Some observations on the scale dependence of permeability by pumping tests," *Water Resources Research*, vol. 42, no. 7, Article ID W07402, 2006.

[4] T. Ouellon, R. Lefebvre, D. Marcotte, A. Boutin, V. Blais, and M. Parent, "Hydraulic conductivity heterogeneity of a local deltaic aquifer system from the kriged 3D distribution of hydrofacies from borehole logs, Valcartier, Canada," *Journal of Hydrology*, vol. 351, no. 1-2, pp. 71–86, 2008.

[5] J. Perrin, B. L. Parker, and J. A. Cherry, "Assessing the flow regime in a contaminated fractured and karstic dolostone aquifer supplying municipal water," *Journal of Hydrology*, vol. 400, no. 3-4, pp. 396–410, 2011.

[6] M. Nastev, M. M. Savard, P. Lapcevic, R. Lefebvre, and R. Martel, "Hydraulic properties and scale effects investigation in regional rock aquifers, south-western Quebec, Canada," *Hydrogeology Journal*, vol. 12, no. 3, pp. 257–269, 2004.

[7] M.-A. Carrier, R. Lefebvre, C. Rivard et al., "Portrait des ressources en eau souterraine en Montérégie Est, Québec, Canada," Projet réalisé conjointement par l'INRS, la CGC, l'OBV Yamaska et l'IRDA dans le cadre du Programme d'acquisition de connaissances sur les eaux souterraines INRS R-1433, 2013.

[8] M. Larocque, S. Gagné, D. Barnetche et al., "Projet de connaissance des eaux souterraines du bassin versant de la zone Nicolet et de la partie basse de la zone Saint-François - Rapport scientifique," Rapport déposé au ministère du Développement durable, de l'Environnement et de la Lutte contre les changements climatiques, 2015.

[9] M. Larocque, S. Gagné, L. Tremblay, and G. Meyzonnat, "Projet de connaissance des eaux souterraines du bassin versant de la rivière Bécancour et de la MRC de Bécancour - Rapport scientifique," Rapport déposé au ministère du Développement durable, de l'Environnement, de la Faune et des Parcs, 2013.

[10] USGS, "Determining Age and Vertical Contribution of Ground Water Pumped from Wells in a Small Coastal River Basin," Tech. Rep. 2005-1032, 2005.

[11] J. L. Libby and G. A. Robbins, "An unsteady state tracer method for characterizing fractures in bedrock wells," *Groundwater*, vol. 52, no. 1, pp. 136–144, 2014.

[12] S. Pistre, S. Marliac, H. Jourde, and P. Bidaux, "New combined log and tracer test interpretation method for identifying transfers in fissured aquifers," *Groundwater*, vol. 40, no. 3, pp. 232–241, 2002.

[13] M. Barahona-Palomo, M. Riva, X. Sanchez-Vila, E. Vazquez-Sune, and A. Guadagnini, "Quantitative comparison of impeller-flowmeter and particle-size-distribution techniques for the characterization of hydraulic conductivity variability," *Hydrogeology Journal*, vol. 19, no. 3, pp. 603–612, 2011.

[14] K. Miyakawa, K. Tanaka, Y. Hirata, and M. Kanauchi, "Detection of hydraulic pathways in fractured rock masses and estimation of conductivity by a newly developed TV equipped flowmeter," *Engineering Geology*, vol. 56, no. 1-2, pp. 19–27, 2000.

[15] F. Paillet, "Borehole flowmeter applications in irregular and large-diameter boreholes," *Journal of Applied Geophysics*, vol. 55, no. 1-2, pp. 39–59, 2004.

[16] A. E. Hess, "Identifying hydraulically conductive fractures with a slow-velocity borehole flowmeter," *Canadian Geotechnical Journal*, vol. 23, no. 1, pp. 69–78, 1985.

[17] M. P. Anderson, "Heat as a ground water tracer," *Groundwater*, vol. 43, no. 6, pp. 951–968, 2005.

[18] G. Ferguson and A. D. Woodbury, "The effects of climatic variability on estimates of recharge from temperature profiles," *Groundwater*, vol. 43, no. 6, pp. 837–842, 2005.

[19] M. Taniguchi, D. R. Williamson, and A. J. Peck, "Disturbances of temperature-depth profiles due to surface climate change and subsurface water flow: 2. An effect of step increase in surface temperature caused by forest clearing in southwest Western Australia," *Water Resources Research*, vol. 35, no. 5, pp. 1519–1529, 1999.

[20] W. S. Keys and R. F. Brown, "The use of temperature logs to trace the movement of injected water," *Groundwater*, vol. 16, no. 1, pp. 32–48, 1978.

[21] R. A. Renken, K. J. Cunningham, A. M. Shapiro et al., "Pathogen and chemical transport in the karst limestone of the Biscayne aquifer: 1. Revised conceptualization of groundwater flow," *Water Resources Research*, vol. 44, no. 8, Article ID W08429, 2008.

[22] M. O. Saar, "Review: geothermal heat as a tracer of large-scale groundwater flow and as a means to determine permeability fields," *Hydrogeology Journal*, vol. 19, no. 1, pp. 31–52, 2011.

[23] G. Ferguson, "Heterogeneity and thermal modeling of ground water," *Groundwater*, vol. 45, no. 4, pp. 485–490, 2007.

[24] D. J. Irvine, C. T. Simmons, A. D. Werner, and T. Graf, "Heat and Solute Tracers: How Do They Compare in Heterogeneous Aquifers?" *Groundwater*, vol. 53, no. 1, pp. 10–20, 2015.

[25] M. V. Klepikova, T. Le Borgne, O. Bour, M. Dentz, R. Hochreutener, and N. Lavenant, "Heat as a tracer for understanding transport processes in fractured media: theory and field assessment from multiscale thermal push-pull tracer tests," *Water Resources Research*, vol. 52, no. 7, pp. 5442–5457, 2016.

[26] M. Chatelier, S. Ruelleu, O. Bour, G. Porel, and F. Delay, "Combined fluid temperature and flow logging for the characterization of hydraulic structure in a fractured karst aquifer," *Journal of Hydrology*, vol. 400, no. 3-4, pp. 377–386, 2011.

[27] T. Le Borgne, F. Paillet, O. Bour, and J.-P. Caudal, "Cross-borehole flowmeter tests for transient heads in heterogeneous aquifers," *Groundwater*, vol. 44, no. 3, pp. 444–452, 2006.

[28] P. E. Pehme, B. L. Parker, J. A. Cherry, J. W. Molson, and J. P. Greenhouse, "Enhanced detection of hydraulically active fractures by temperature profiling in lined heated bedrock boreholes," *Journal of Hydrology*, vol. 484, pp. 1–15, 2013.

[29] V. F. Bense, T. Read, O. Bour et al., "Distributed Temperature Sensing as a downhole tool in hydrogeology," *Water Resources Research*, vol. 52, no. 12, pp. 9259–9273, 2016.

[30] M. V. Klepikova, T. Le Borgne, O. Bour, and P. Davy, "A methodology for using borehole temperature-depth profiles under ambient, single and cross-borehole pumping conditions to estimate fracture hydraulic properties," *Journal of Hydrology*, vol. 407, no. 1-4, pp. 145–152, 2011.

[31] M. V. Klepikova, T. Le Borgne, O. Bour, K. Gallagher, R. Hochreutener, and N. Lavenant, "Passive temperature tomography experiments to characterize transmissivity and connectivity of preferential flow paths in fractured media," *Journal of Hydrology*, vol. 512, pp. 549–562, 2014.

[32] M. J. Drury and A. M. Jessop, "The effect of a fluid-filled fracture on the temperature profile in a borehole," *Geothermics*, vol. 11, no. 3, pp. 145–152, 1982.

[33] S. Ge, "Estimation of groundwater velocity in localized fracture zones from well temperature profiles," *Journal of Volcanology and Geothermal Research*, vol. 84, no. 1-2, pp. 93–101, 1998.

[34] Y. Globensky, "Géologie des Basses-Terres du Saint-Laurent," Tech. Rep. MM85-02, Direction Générale de L'exploitation Géologique et Minérale, Québec, Canada, 1987.

[35] M. Larocque and G. Meyzonnat, "Projet de connaissance des eaux souterraines de la zone de Vaudreuil-Soulanges - Rapport scientifique," Rapport déposé au ministère du Développement durable, de l'Environnement et de la Lutte contre les changements climatiques, 2015.

[36] Terraplus, QL 40 SFM, bidirectionnal spinner flowmeter, User guide, Richmond Hill, ON, Canada, 2014.

[37] Terraplus, Matrix Borehole Logging System, User guide, Richmond Hill, ON, Canada, p. 2, 2014.

[38] Terraplus, QL-40 OBI, optical borehole imager, User guide, Richmond Hill, ON, Canada, p. 2, 2014.

[39] F. Barbecot, C. Marlin, E. Gibert, and L. Dever, "Hydrochemical and isotopic characterisation of the Bathonian and Bajocian coastal aquifer of the Caen area (northern France)," *Applied Geochemistry*, vol. 15, no. 6, pp. 791–805, 2000.

[40] J.-A. Corcho Alvarado, F. Barbecot, and R. Purtschert, "Ambient vertical flow in long-screen wells: a case study in the Fontainebleau Sands Aquifer (France)," *Hydrogeology Journal*, vol. 17, no. 2, pp. 425–431, 2008.

[41] A. Faghri, Y. Zhang, and J. R. Howell, *Advanced Heat and Mass Transfer*, Global Digital Press, Missouri, MO, USA, 2010.

[42] B. L. Kurylyk and D. J. Irvine, "Analytical solution and computer program (FAST) to estimate fluid fluxes from subsurface temperature profiles," *Water Resources Research*, vol. 52, no. 2, pp. 725–733, 2016.

[43] Terraplus, HFP-2293, heat-pulse Flowmeter probe, User guide, Richmond Hill, ON, Canada, p. 2, 2014.

[44] C. Gosselin and J.-C. Mareschal, "Recent warming in northwestern Ontario inferred from borehole temperature profiles," *Journal of Geophysical Research: Solid Earth*, vol. 108, no. 9, 2003.